Evaluation of PGM2007A by comparison with globally and locally estimated gravity solutions from CHAMP

M. Weigelt, N. Sneeuw, W. Keller
Geodätisches Institut,
Universität Stuttgart, Geschwister-Scholl-Str. 24D, 70174 Stuttgart, Germany

Abstract. New gravity field models incorporate GRACE data as the best available data source for the low to medium wavelength but validation is difficult since comparisons with existing GRACE models will always be biased. Maybe the best independent data set on a global scale is therefore the CHAMP data. It is known that the accuracy of the CHAMP solutions is approximately one order of magnitude worse than the one of GRACE-only solutions. On the other hand and considering e.g. the degree difference RMS between PGM2007A and GGM02S, also discrepencies between these models occur which cannot solely be explained by numerical inaccuracies. Consequently, it has been investigated if the CHAMP solutions can serve as an indicator. This research shows results of the evaluation of the preliminary gravity field model PGM2007A with a CHAMP solution derived from two years of kinematic orbits. The quality of the global CHAMP solutions is further improved by a local refinement with Slepian functions which can make better use of the information in areas of high data density, e.g. in high-latitude areas. However, it is concluded that despite the data density the poorer quality of the CHAMP data is preventing a definite assessment of the quality of the PGM2007A.

Keywords. CHAMP, GRACE, energy balance approach, spherical harmonics, Slepian functions

1 Introduction

The evaluation of the preliminary gravity field model PGM2007A with CHAMP data will focus on the low to medium degree part of the spectrum due to the restricted spatial and spectral resolution of the CHAMP mission. It is a comparison between a single satellite but independent solution and PGM-2007A which contains besides GRACE also altimetric and terrestrial data. Three different data sets will be considered in the comparison. Besides PGM-2007A, the GRACE-only solution GGM02S provided by UTCSR (*Tapley et al.*, 2005) and a two year CHAMP-only solution (*Weigelt*, 2007) is used.

Before we start with the description of the data processing and the validation approach, all statistical quantities used throughout the paper are stated in section 2 for the sake of completeness. Section 3 introduces a short review of the CHAMP data processing strategy. The primary measurements are positions, velocities and accelerations which need to be related to a gravity field quantity. For this, the so-called energy balance approach is used in order to derive pseudo-potential observations along the orbit (*Jacobi*, 1836; *Jekeli*, 1999; *Gerlach et al.*, 2003). Subsequently, a global spherical harmonic analysis is performed in order to derive the global satellite-only solution. Since the data is not equally distributed, a local refinement in areas with high data density can make better use of the available information (*Garcia*, 2002; *Weigelt*, 2007). Here, the Slepian functions are employed and a proof of concept is presented in section 3.3.2. Subsequently, section 4 presents the global and local validation results in an attempt to indicate whether the CHAMP data agrees better with PGM2007A or GGM02S.

2 Tools of analysis

The quantification of the differences between CHAMP, GGM02S and PGM2007A is done in term of statistical quantities. For completeness, all the necessary formulas are given here with short explanations. They will be used extensively in section 4.

2.1 Spatial domain

Besides the maxima and minimum values and their location, values of interest are the mean, the standard deviation and the root mean square (RMS), arithmetic as well as area-weighted. The mean is given as:

$$\text{arithmetic:} \qquad \mu = \frac{1}{N}\sum_{i=1}^{N} x_i \tag{1}$$

$$\text{area weighted:} \qquad \mu_w = \frac{\sum_{i=1}^{N} w_i \cdot x_i}{\sum_{i=1}^{N} w_i}, \tag{2}$$

where x_i are the observations, N the number of observations and w_i the weights which are here determined

by calculating the area of a Voronoi cell around each data point. A Voronoi cell is characterized by an area in which any point is closer to the data point than to any neighboring data point. It is also referred to as Thiessen-polygons, Voronoi diagram or Dirichlet decomposition (*Barber et al.*, 1996).

The standard deviation is defined as the square root of the second moment of the mean, i.e. the square root of the variance:

$$\text{arithmetic:} \qquad \sigma = \sqrt{\frac{1}{N}\sum_{i=1}^{N}(x_i-\mu)^2} \tag{3}$$

$$\text{area weighted:} \qquad \sigma_w = \sqrt{\frac{\sum_{i=1}^{N} w_i \cdot (x_i-\mu_w)^2}{\sum_{i=1}^{N} w_i}}. \tag{4}$$

The RMS is defined very similar:

$$\text{arithmetic:} \qquad \text{RMS} = \sqrt{\frac{1}{N}\sum_{i=1}^{N}x_i^2} \tag{5}$$

$$\text{area weighted:} \qquad \text{RMS}_w = \sqrt{\frac{\sum_{i=1}^{N} w_i \cdot x_i^2}{\sum_{i=1}^{N} w_i}}. \tag{6}$$

In case of a zero mean, standard deviation and RMS will coincide.

Two, more rarely, used quantities are the skewness and kurtosis (*Webster and Oliver*, 2001). The skewness coefficient is defined formally as the third momentum of the mean divided by the third power of the standard deviation:

$$g = \frac{1}{\sigma^3}\cdot\frac{1}{N}\sum_{i=1}^{N}(x_i-\mu)^3. \tag{7}$$

It is a measure of the asymmetry of the observations. Symmetric distributions have $g = 0$. Comparisons between means of different data sets are unreliable if the data is skewed. The kurtosis gives an estimate of the peakedness of a distribution:

$$k = \frac{1}{\sigma^4}\cdot\frac{1}{N}\sum_{i=1}^{N}(x_i-\mu)^4. \tag{8}$$

For normal distributions $k = 0$; flatter distributions have $k < 0$ and more peaked ones $k > 0$.

2.2 Spectral domain

The spherical harmonic coefficients $\bar{K}_{lm}$ are two-dimensional quantities which are derived, e.g. in a least-squares adjustment or by quadrature. As output, the covariance matrix of the unknowns $Q_{\hat{x}\hat{x}}$ might be available. Taking the diagonal elements, the variance of the coefficients can be represented but correlations are neglected.

$$\text{diag}\,(Q_{\hat{x}\hat{x}}) = \text{VAR}\,\{\bar{K}_{lm},\bar{K}_{lm}\} = \sigma_{lm}^2 \tag{9}$$

The variance primarily represents the internal accuracy of the estimation, i.e. the fit of the model to the data. For a comparison with external data the difference between two signal spectra is more adequate:

$$\Delta_{lm} = \bar{K}_{lm}^2 - \bar{K}_{lm}^1. \tag{10}$$

The advantage of the latter is that it can also be used when $Q_{\hat{x}\hat{x}}$ is not available. Both of them are two-dimensional representations of signal and noise.

The most common way to determine a one-dimensional error spectrum from spherical harmonic coefficients is to derive degree-specific quantities. The first one to be mentioned is the error degree variance:

$$\sigma_l^2 = \sum_{m=-l}^{l}\sigma_{lm}^2 \qquad \forall \quad l \in [2\ldots L]. \tag{11}$$

The summation in this case is from $-l$ to l, where the negative degrees denote the sine and the positive the cosine coefficients. The error degree variance represents the total error power in the coefficients per degree and is a quadratic quantity. Dividing it by the number of coefficients $(2l+1)$ and taking the square root, an average standard deviation for the coefficients of a specific degree l can be derived. The result is the root mean square of the error spectrum per degree:

$$\text{RMS}_l = \sqrt{\frac{\sigma_l^2}{2l+1}} = \sqrt{\frac{1}{2l+1}\sum_{m=-l}^{l}\sigma_{lm}^2}. \tag{12}$$

The RMS_l is a representative standard deviation if and only if the error spectrum is isotropic, i.e. it is independent of the order m. Order specific components can also be derived but do not have any physical meaning. Equations (11) and (12) can be applied analogously to the signal difference spectrum (equation 10) yielding difference degree variances and difference degree RMS. These quantities will be used in the discussion of the global solutions in section 4.1.

3 Data Processing

The gravity field from CHAMP-data is recovered using the energy balance approach which yields pseudo-potential observations along the orbit (cf. section 3.1), followed by a brute-force spherical harmonic analysis on the sphere, see section 3.2. More details about the data processing can be found in *Weigelt* (2007). In section 3.3, we show that a local refinement could provide additional information in selected areas and introduce the framework of a Slepian analysis.

3.1 Energy balance approach

The basic idea is to separate orbit determination and gravity field recovery into three steps. The first step is the derivation of the position data which is done kinematically and provided by the Institute for Astronomical and Physical Geodesy (IAPG), TU Munich (*Švehla and Rothacher*, 2005). The data is considered independent from a priori information because no dynamical model is used in the calculation. Since the kinematic derivation yields positions only, velocities have to be derived numerically by a 4^{th} order central difference Taylor differentiator (*Khan and Ohba*, 1999). Subsequently, pseudo-potential observations are derived from the position data. The utilized energy balance approach is based on the law of energy conservation. The basic formula is given as:

$$T = E^{\text{kin}} - U - Z - \int \left(\mathbf{f} + \sum_i \mathbf{g}_i \right) d\mathbf{x} + c, \quad (13)$$

where T is the disturbing, U the normal and Z the centrifugal potentials. The latter two can be calculated pointwise from the position data. The normal potential is derived from the $WGS84$-constants which are given in table 1. The kinetic energy E^{kin} is derived from the velocity of the satellite. The integral contains all known time-variable gravitational accelerations $\mathbf{g}_i$ which are derived from models and are summarized in table 2. Non-gravitational accelerations $\mathbf{f}$ are measured using the accelerometer onboard CHAMP and calibration parameters are determined together with the integration constant c using a comparison of the pseudo-observables with the disturbing potential along the orbit derived from a known *a priori* model (here EGM96). Necessary transformations between the Earth-fixed and inertial frame are done in accordance with the IERS Conventions 2003 (*McCarthy and Petit*, 2003). Overall, two years of data from April 2002 till February 2004 are used for the calculation.

Tbl. 1. Constants in the calculation

	name	value
GM	grav. parameter	$3.986004415 \cdot 10^{14}\,\mathrm{m^3/s^2}$
R	radius	$6378136.46\,\mathrm{m}$
J_2	SH-coefficient	$1.08262982131 \cdot 10^{-03}$
J_4	SH-coefficient	$-2.37091120053 \cdot 10^{-06}$
J_6	SH-coefficient	$6.08346498882 \cdot 10^{-09}$
J_8	SH-coefficient	$-1.42681087920 \cdot 10^{-11}$
ω	rotation rate	$7.292115085 \cdot 10^{-05}\,\mathrm{rad/s}$

Tbl. 2. Utilized models for known corrections

source	model
astronomic tide	Sun/Moon (point masses) coordinates from DE405
solid Earth tide	IERS Conv. 2003, §6.1
solid Earth pole tide	IERS Conv. 2003, §6.2
ocean tide	FES2004
ocean pole tide	IERS Conv. 2003, §6.3
relativistic corrections	IERS Conv. 2003, §10.2

3.2 Global spherical harmonic analysis

The spherical harmonic analysis with its inherent downward continuation is done using a least-squares approach. The mathematical model connecting the pseudo-observable T with the spherical harmonic coefficients is given as:

$$T(r,\theta,\lambda) = \frac{GM}{R} \sum_{l=2}^{\infty} \sum_{m=-l}^{l} \left(\frac{R}{r} \right)^{l+1} \bar{K}_{lm} \bar{Y}_{lm}, \quad (14)$$

where G is the gravitational constant, M the mass of the Earth, R the radius, r, θ and λ the spherical coordinates of the calculation point, $\bar{K}_{lm}$ the fully normalized spherical harmonic coefficients and $\bar{Y}_{lm}$ the spherical surface harmonics. The indices of the double summation are the degree l and the order m. For the least squares adjustment the equation can be reorganized into matrix-vector form:

$$\mathbf{l} + \varepsilon = A\mathbf{x}, \quad (15)$$

where $\mathbf{l}$ is the observation vector and is filled with the observations T. It is a stochastic quantity, which is expressed by the model inconsistencies ε. The unknown vector $\mathbf{x}$ is formed by the spherical harmonic coefficients $\bar{K}_{lm}$. All other elements of equation (14) are part of the A-matrix, i.e. for one particular mea-

surement k an element j of A reads:

$$a_{kj} = \frac{GM}{R}\left(\frac{R}{r}\right)^{n_j+1} P_{n_j,m_j}(\cos\theta_k)e^{im_j\lambda_k}. \quad (16)$$

The factor j denotes the column of the design matrix A and stands for a coefficient with one specific combination of degree l and order m. Here, the ordering is in accordance with *Colombo* (1983) which collectes $\bar{C}_{lm}$- and $\bar{S}_{lm}$-coefficients for all degrees in blocks of ascending orders. As an example and considering a maximum degree of $L = 70$, the column $j = 3$ corresponds to $\bar{C}_{20}$, $j = 73$ to $\bar{C}_{21}$ and $j = 143$ to $\bar{S}_{21}$. The least-squares solution is then achieved as:

$$\hat{x} = \underbrace{\left(A^T PA\right)^{-1}}_{N^{-1}} \underbrace{A^T Pl}_{y} = N^{-1}y, \quad (17)$$

where P is the inverse of the cofactor matrix and contains the error information of the observations. The kinematic positions are provided with error information for each data point including correlations between the coordinates but different data points are assumed uncorrelated.

3.3 Local refinement with Slepian functions

The motivation for a local refinement comes from the investigations by *Sneeuw et al.* (2003) who showed among others that the data distribution and the groundtrack influence the accuracy of the monthly CHAMP solutions. A similar effect for the GRACE-mission was discussed by *Yamamoto et al.* (2005) and *Wagner et al.* (2006). It is also known that the orbits are converging towards the poles yielding a much higher data density in these areas. Figure 1 shows the number of data points in 100 km^2 patches vs. the latitude. The increase of the data points per area is clearly visible. Consequently and by utilizing locally supported base functions, one can make better use of the information in the high-latitude areas.

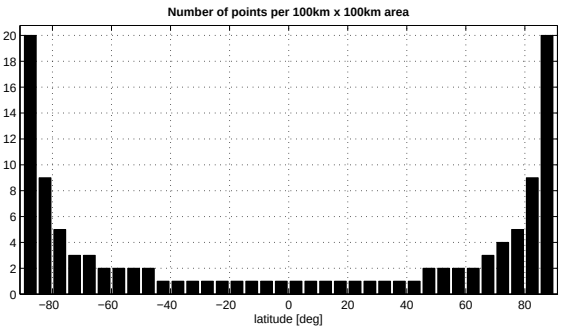

Fig. 1. Number of points per 100 km^2 area vs. latitude

3.3.1 An empirical localizing base function

Consider a function f which is strictly contained within an arbitrarily shaped region ω on the sphere Ω. Since it will not have values outside this area, it is spacelimited. Nevertheless and as any function on a sphere, it can be described by an infinite spherical harmonic expansion:

$$f = \sum_{l=0}^{\infty}\sum_{m=-l}^{l} \bar{f}_{lm}\bar{Y}_{lm}, \quad (18)$$

where $\bar{Y}_{lm}$ are again the spherical surface harmonics and $\bar{f}_{lm}$ the spherical harmonic coefficients, both normalized. Practically, a series till infinity cannot be implemented and the series needs to be truncated at a maximum degree L. The function becomes bandlimited.

Strictly speaking, no spherical function can be spacelimited and bandlimited at the same time. However, a set of bandlimited functions can be found, which are optimally concentrated within the area ω, and vice versa a spacelimited function, which is optimally concentrated within an interval $0 \le l \le L$. *Gilbert and Slepian* (1977) showed that this leads to the same description as an algebraic eigenvalue problem. The basic idea is to maximize the ratio between the spacelimited and the unlimited norm and thus the spatial concentration of the bandlimited function:

$$\xi = \frac{\|f\|_\omega^2}{\|f\|_\Omega^2} = \frac{\int\limits_\omega f^2\, d\Omega}{\int\limits_\Omega f^2\, d\Omega}, \quad (19)$$

where ξ is a measure of the spatial concentration. Using the bandlimited spherical harmonic synthesis formula and making use of the orthonormality relation of the normalized spherical surface harmonics, the relation reads

$$\xi = \frac{\sum\limits_{l=0}^{L}\sum\limits_{m=-l}^{l} \bar{f}_{lm}\sum\limits_{n=0}^{L}\sum\limits_{k=-n}^{n} D_{lmnk}\bar{f}_{nk}}{\sum\limits_{l=0}^{L}\sum\limits_{m=-l}^{l} \bar{f}_{lm}^2}, \quad (20)$$

with

$$D_{lmnk} = \int\limits_\omega \bar{Y}_{lm}\bar{Y}_{nk}\, d\Omega. \quad (21)$$

The elements D_{lmnk} can be arranged in a matrix D which is real, symmetric and positive definite. The solution of the spatial localization problem is found as the solution of an algebraic eigenvalue problem

forming an orthogonal set of base functions (*Simons et al.*, 2005):

$$D = G \Xi G^T. \tag{22}$$

Each column $\bar{g}^j$ of G represents an eigenvector and forms a base function $\bar{S}_j$ which can be reconstructed by

$$\bar{S}_j(\lambda,\theta) = \sum_{l=0}^{L} \sum_{m=-l}^{l} \bar{g}^j_{lm} \bar{Y}_{lm}(\lambda,\theta). \tag{23}$$

The corresponding eigenvalue ξ^j indicates the spatial concentration in the area R. Using the fully normalized Legendre functions for the calculation of D_{lmnk}, the eigenvalues will be normalized. $\xi = 1$ represents an optimal and $\xi = 0$ no concentration in the area of interest.

The application of the Slepian functions in physical geodesy is also not new. *Albertella et al.* (1999) considered the Slepian functions as a possible solution to the polar gap problem. Similar to equation (14), the potential along the orbit can be developed in Slepian base functions:

$$T(r,\theta,\lambda) = \frac{GM}{R} \sum_{j=1}^{(L+1)^2} \bar{\beta}_j \bar{S}_j(\lambda,\theta,r) \tag{24}$$

The unknown coefficients $\bar{\beta}_j$ are to be determined in a least-squares adjustment. Practically, not all $(L+1)^2$ Slepian coefficients can be estimated when utilizing local data. Only those with a concentration of 99% or higher will be considered since only those are well supported by the data. Less concentrated base functions will either cause leakage errors or lead to a rank deficient design matrix.

3.3.2 Proof of concept

The concept is proven in a test scenario with real CHAMP data of January 2003. GGM02S will serve as a reference for the comparison of the global spherical harmonic solution and Slepian solution. All solutions as well as the development of the kernel D_{lmnk} and the Slepian base functions are restricted to degree 70. The area of interest is a 23.5° spherical cap over Canada. Since only local data is to be used for the refinement, the long wavelength part cannot be estimated and needs to be reduced beforehand. For this, a global spherical harmonic solution till degree and order 40 has been derived from the data of January 2003 and reduced. After the estimation of the parameter $\bar{\beta}_j$, equation (24) can be used to synthesis the data in the area of interest and compare the results in the spatial domain with GGM02S.

The statistics of the comparison are shown in table 3 and indicate that by the usage of the Slepian functions an improvement has been reached. The maximum and minimum values are reduced by approximately 40% from 4.03 m to 2.39 m and from −3.76 m to −2.21 m, respectively. Since the mean value is close to zero, standard deviation and RMS are almost identical but both are reduced by 42.3% in case of the Slepian solution. The skewness indicates that the differences of the Slepian solution are slightly more asymmetric. Nevertheless, the values for both solutions are close to zero, i.e. the data can be considered unskewed and thus the comparison of the mean values is valid. The kurtosis shows a slightly flatter solution in case of the Slepian func-

Tbl. 3. Statistics of the differences of the global monthly spherical harmonic solution and the Slepian solution to GGM02S in terms of geoid height

quantity	global SH	Slepian
maximum	4.03 m	2.39 m
at $\lambda =$	110.62° W	60.62° W
$\phi =$	52.71° N	45.63° N
minimum	−3.76 m	−2.21 m
at $\lambda =$	106.87° W	106.04° W
$\phi =$	49.38° N	79.38° N
μ	-0.015 m	-0.011 m
μ_w	-0.020 m	-0.015 m
σ	1.384 m	0.855 m
σ_w	1.404 m	0.873 m
RMS	1.383 m	0.856 m
RMS_w	1.404 m	0.873 m
g	-0.026	0.110
k	-0.170	-0.271

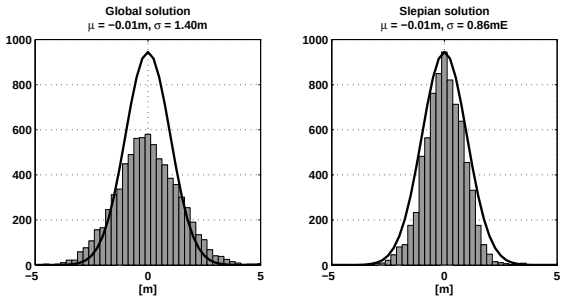

Fig. 2. Histogram of the monthly spherical harmonic solution (left) and the Slepian solution (right) vs. GGM02S in terms of geoid height

tions, i.e. peaks in this solution are flatter than in the global spherical harmonic solution. Practically, there is also no difference between the arithmetic and the area-weighted quantities which suggests that the differences are normally distributed. However, the histograms of both comparisons in figure 2 show that the data in the Slepian solution is closer to be normally distributed than the data of the global spherical harmonic solution.

Figure 3 visualizes the comparison in the spatial domain in terms of geoid height. The differences of the spherical harmonic solution (top) grows with increasing latitude and are more pronounced than the one of the Slepian solution (bottom). The pattern appears to be similar but in the later case the absolute values are approximately half the size of the former.

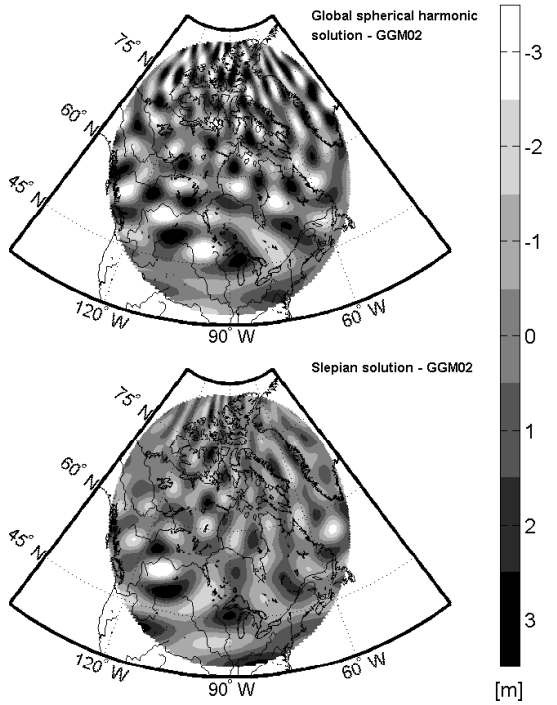

Fig. 3. Difference of the monthly spherical harmonic solution (top) and the Slepian solution (bottom) w.r.t. GGM02S in terms of geoid height

The results show that the improvement is primarily due to a better modelling of the short wavelength part of the spectrum and it can be concluded that better use of the data can be made by a local refinement. In the shown case, the global spherical harmonic analysis is obviously not able to take full advantage of the data density in the high-latitude area.

4 Validation results

After having outlined the data processing and the validation tools, this section will deal with the actual validation of the gravity field model PGM2007A. Naturally, both PGM2007A and GGM02S will outperform the CHAMP solution due to the higher data quality, i.e. a comparison in terms of absolute values does not make sense. Instead, the idea is to use the CHAMP solution as an indicatior by comparing the differences to PGM2007A and GGM02S in the spectral and spatial domain. Consequently, it can only be concluded to which model the CHAMP data fits better.

4.1 Global comparisons

The first comparison is done in the spectral domain. Figure 4 shows error and difference degree RMS of the three different solutions. The bottom

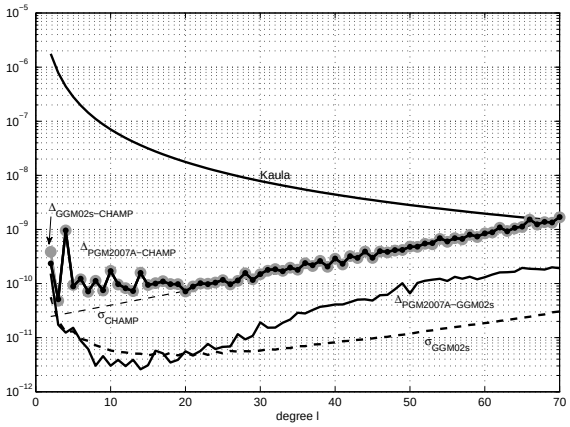

Fig. 4. Error and difference spectra of GGM02S, PGM-2007A and the CHAMP-solution

black solid line shows the difference degree RMS between PGM2007A and GGM02S whereas the dashed black line indicates the error degree RMS of GGM02S. Note the significant discrepancy. For the very low degrees, the difference degree spectrum is following the GGM02S error spectrum but from degree 20 onwards the difference deviates up to one order of magnitude.

The question is if CHAMP can serve now as an indicator. The gray and black line with dot marks are the difference degree RMS between GGM02S and PGM2007A both w.r.t. CHAMP. They are almost identical with the exception of degree 2. Here, the PGM2007A and the GGM02S solution disagree slightly which might be related to the handling of the $\bar{C}_{21}$- and $\bar{S}_{21}$-coefficients. Obviously and for all

degrees, the difference between PGM2007A and GGM02S is smaller than the difference to CHAMP and thus drawing conclusions will be very difficult. It is a first indication that both fields will perform equally in the comparison to the CHAMP data.

The comparison to the CHAMP data in the spatial domain and on a global scale is shown in figure 5 but it is inconclusive. Both solutions show no significantly different pattern. The statistical data and the histograms support this. The most significant difference is in the extreme values. The maximum differs with 1.342 m for GGM02S and 1.326 m for PGM-2007A by 1.6 cm. However, their location is varying and, considering the random nature of the differences in figure 5, this cannot be seen as significant. On the other hand, the minima with -1.338 m for GGM02S and -1.364 m for PGM2007A are at the same location and differ by 2.6 cm and thus show a very slight tendency of the CHAMP data towards the GGM02S solution. Mean value, standard deviation and RMS have the same slight tendency as the minimum but on average the difference for the latter two is 4 mm which is approximately 1% of the signal and thus cannot be considered significant. The skewness shows the difference between GGM02S and CHAMP is slightly more symmetric and the kurtosis indicates that it is also slightly less peaked than the difference between PGM2007A and CHAMP.

Overall, it has to be concluded that the differences are not significant and the GGM02S as well as the PGM2007A solution show the same behavior in the comparison to the CHAMP data. At best, one can say that there is a very slight tendency of the CHAMP data towards the GGM02S-solution.

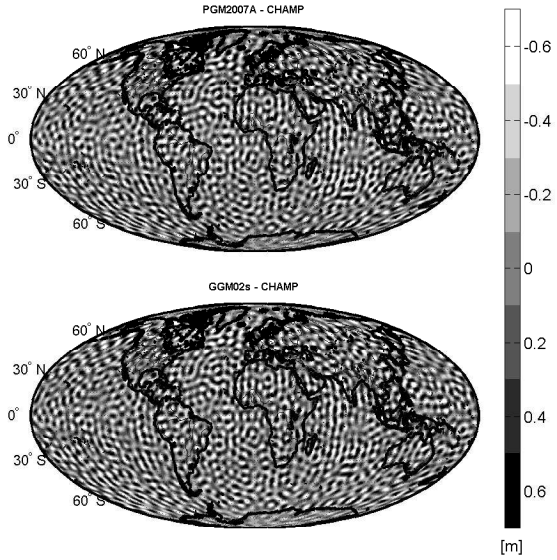

Fig. 5. Spatial comparison between the GGM02S and PGM2007A solution w.r.t. the global CHAMP solution

Tbl. 4. Statistics of the differences of GGM02S and PGM2007A to the CHAMP solution in terms of geoid height

quantity	PGM2007A	GGM02S
maximum	1.326 m	1.342 m
at λ	77.00° E	72.00° E
ϕ	29.00° N	22.00° S
minimum	-1.364 m	-1.338 m
at λ	19.00° E	19.00° E
ϕ	52.00° S	52.00° S
μ	-0.018 m	-0.004 m
μ_w	-0.024 m	-0.009 m
σ	0.320 m	0.317 m
σ_w	0.329 m	0.326 m
RMS	0.321 m	0.317 m
RMS_w	0.330 m	0.326 m
g	0.038	0.029
k	0.239	0.199

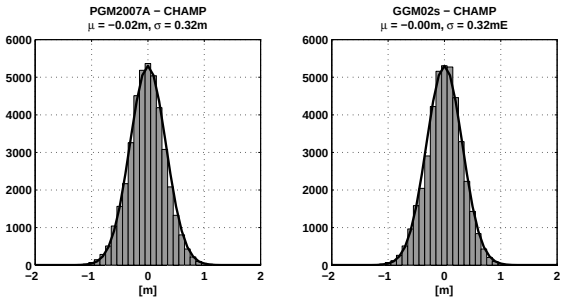

Fig. 6. Histogram of PGM2007A (left) and GGM02S (right) w.r.t. the CHAMP soluition in terms of geoid height

4.2 Local comparison

For the local refinement of the CHAMP solution a latitude band from 60° N to 85° N is chosen and 141 base functions are used in the Slepian adjustment to improve the solution. In the remove step the full global spherical harmonic solution from CHAMP till degree 70 is used. The recovered residual signal has a strength of $\delta N \approx 10$ cm which is added in the spatial domain to the spherical harmonic solution

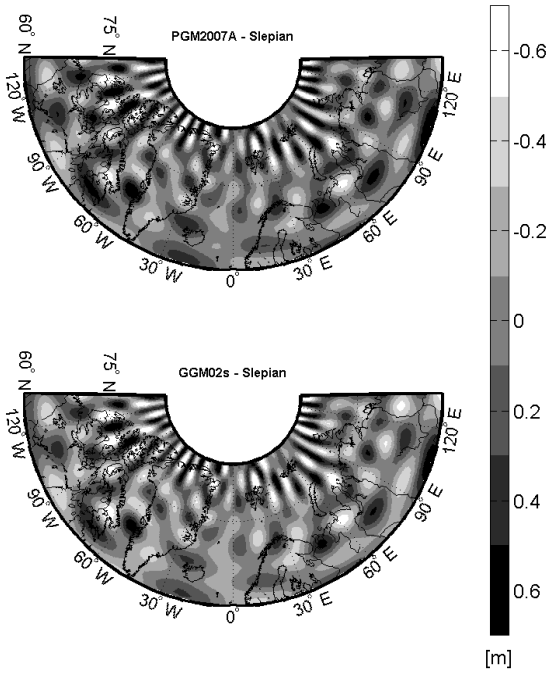

Fig. 7. Spatial comparison between the PGM2007A (top) and GGM02S (bottom) solution w.r.t. the CHAMP solution for a latitude band from 60° N to 85° N

and hereafter called the Slepian solution.

The comparison in the spatial domain of PGM-2007A and GGM02S to the Slepian solution is shown in figure 7 but again shows no significant differences. The top picture, i.e. the comparison between PGM2007A and the Slepian solution, appears slightly darker but both pictures are dominated by the deficiencies in the CHAMP data.

The histograms show nearly identical values for both cases. The difference between PGM2007A and the Slepian solution has a by 2 cm higher mean value

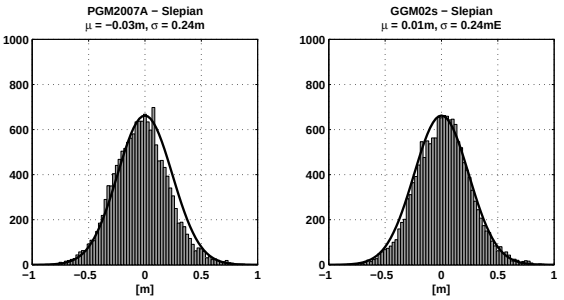

Fig. 8. Histogram of GGM02S and PGM2007A solution w.r.t. the Slepian solution for a latitude band from 60° N to 85° N

which explains the darker impression of the top panel in figure 7. The extremas of both solutions are at the same location and thus comparable. The maximum values are 1.014 m for GGM02S and 1.032 m for PGM2007A and differ by 1.8 cm. The minimum values are −1.207 m for GGM02S and −1.217 m for PGM2007A and thus 1 cm smaller in the difference of the GGM02S to the Slepian solution, i.e. there is again a slight tendency of the CHAMP data towards the GRACE solution. The same can be seen in the mean value. All other statistics are very similar and the differences are not significant.

Tbl. 5. Statistics of the differences of PGM2007A and GGM02S to the CHAMP solution in terms of geoid height for a latitude band from 60° N to 85° N

quantity	PGM2007A	GGM02S
maximum	1.032 m	1.014 m
at λ	89.38° W	89.38° W
ϕ	66.88° N	66.88° N
minimum	−1.217 m	−1.207 m
at λ	176.88° W	176.88° W
ϕ	61.88° N	61.88° N
μ	-0.030 m	-0.006 m
μ_w	-0.031 m	-0.015 m
σ	0.247 m	0.245 m
σ_w	0.318 m	0.313 m
RMS	0.247 m	0.245 m
RMS_w	0.318 m	0.314 m
g	-0.0347	-0.0378
k	0.5799	0.6098

5 Conclusions

In conclusion, one can say that the poorer quality of the CHAMP data is preventing a real statement about the quality of the PGM2007A. At best, one can say that the global as well as the local CHAMP solution agree slightly better with the GRACE-only solution GGM02S than with the PGM2007A. PGM2007A and GGM02S show significant difference from degree 20 to 70 which, however, cannot be verified nor quantified in the comparison to the CHAMP data.

Acknowledgements We like to acknowledge Drazen Švehla from the Institute of Astronomical and Physical Geodesy, TU Munich, for providing the kinematic position data for CHAMP and GFZ Pots-

dam for providing the acceleration data. We also appreciate the comments of the reviewer Dr. Thomas Gruber from the Institute of Astronomical and Physical Geodesy, TU Munich, which helped clarifying the content of the paper.

References

Albertella, A., F. Sansò, and N. Sneeuw, Band-limited functions on a bounded spherical domain: the Slepian problem on the sphere, *Journal of Geodesy*, *73*, 436–447, 1999.

Barber, C., D. Dobkin, and H. Huhudanpaa, The Quickhull Algorithm for Convex Hulls, *ACM Transactions on Mathematical Software*, *22*, 469–483, 1996.

Colombo, O., Numerical methods for harmonic analysis on the sphere, *Tech. rep.*, Report No.310, Dept. Geod. Sci. and Surv., Ohio State Univ., Columbus, Ohio, 1983.

Garcia, R., Local geoid determination from GRACE, Ph.D. thesis, Ohio State University, 2002.

Gerlach, C., N. Sneeuw, P. Visser, and D. Švehla, CHAMP gravity field recovery using the energy balance approach, *Advances in Geosciences*, *1*, 73–80, 2003.

Gilbert, E., and D. Slepian, Doubly Orthogonal Concentrated Polynomials, *SIAM Journal on Mathematical Analysis*, *8*, 290–319, 1977.

Jacobi, C., Über ein neues Integral für den Fall der drei Körper, wenn die Bahn des störenden Planeten kreisförmig angenommen und die Masse des gestörten vernachlässigt wird., *Monthly reports of the Berlin Academy*, 1836.

Jekeli, C., The determination of gravitational potential differences from satellite-to-satellite tracking, *Celestial Mechanics and Dynamical Astronomy*, *75*, 85–101, 1999.

Khan, I., and R. Ohba, Closed-form expressions for the finite difference approximations of first and higher derivaties based on Taylor series, *Journal of Computational and Applied Mathematics*, *107*, 179–193, 1999.

McCarthy, D. D., and G. Petit, IERS conventions 2003, *Tech. Rep. 32*, IERS, Frankfurt am Main, Verlag des Bundesamts für Kartographie und Geodäsie, 2003, updated version from 20th July 2006.

Simons, F., F. Dahlen, and M. Wieczorek, Spatiospectral concentration on a sphere, *Siam Reviews*, 2005.

Sneeuw, N., C. Gerlach, D. Švehla, and C. Gruber, A first attempt at time-variable gravity field recovery from CHAMP using the energy balance approach, in *Gravity and Geoid 2002*, edited by I. Tziavos, Proceedings of 3rd Meeting of the International Gravity and Geoid Commission, pp. 237–242, Editions ZITI, Thessaloniki, Greece, 2003.

Švehla, D., and M. Rothacher, Kinematic precise orbit determination for gravity field determination, in *A window on the future of geodesy*, edited by F. Sansò, vol. 128 of *International Association of Geodesy Symposia*, Springer, 2005.

Tapley, B., J. Ries, S. Bettadpur, D. Chambers, M. Cheng, F. Condi, B. Gunter, Z. Kang, P. Nagel, R. Pastor, T. Pekker, S. Poole, and F. Wang, GGM02 - An improved Earth gravity field model from GRACE, *Journal of Geodesy*, *79*, 467 – 478, 2005.

Wagner, C., D. McAdoo, J. Klokočník, and J. Kostelecký, Degradation of geopotential recovery from short repeat-cycle orbits: application to GRACE monthly fields, *Journal of Geodesy*, *80*, 94–103, 2006.

Webster, R., and M. Oliver, *Geostatistics for enviromental scientists*, Statistics in Practice, J.Wiley & sons, LTD, 2001.

Weigelt, M., Global and local gravity field recovery from satellite-to-satellite tracking, Ph.D. thesis, University of Calgary, http://www.geomatics.ucalgary.ca/graduatetheses, 2007.

Yamamoto, K., T.Otsubo, T. Kubo-oka, and Y. Fukuda, A simulation study of effects of GRACE orbit decay on the gravity field recovery, *Earth Planets Space Letter*, *57*, 291 – 295, 2005.